Supplement of Atmos. Chem. Phys., 20, 12697–12719, 2020
https://doi.org/10.5194/acp-20-12697-2020-supplement
© Author(s) 2020. This work is distributed under
the Creative Commons Attribution 4.0 License.

Atmospheric Chemistry and Physics
Open Access
EGU

Supplement of

Vertical variability of the properties of highly aged biomass burning aerosol transported over the southeast Atlantic during CLARIFY-2017

Huihui Wu et al.

Correspondence to: Hugh Coe (hugh.coe@manchester.ac.uk)

The copyright of individual parts of the supplement might differ from the CC BY 4.0 License.

S1 The calculation of enhancement ratios and MCE

The enhancement ratios (ER) of BC and OA can be calculated by dividing them by the excess concentration of CO, after backgrounds have been removed (Lefer et al., 1994). The modified combustion efficiency (MCE) is defined as the excess mixing ratio of CO_2 over the background to the sum of the excess mixing ratio of CO and CO_2: MCE = $\Delta CO_2/(\Delta CO+\Delta CO_2)$ (Yokelson et al., 2009). For an identified smoke, MCE can be calculated by determining the slope between CO and CO_2 using an unconstrained linear orthogonal distance regression (ODR) and subsequently solving for MCE = $1/(1+\delta CO/\delta CO_2)$. BC/ΔCO can be also calculated by determining the slope between BC and CO using the unconstrained linear ODR, the same for OA/ΔCO. However, when plumes are mixed into different air masses background values may change and this can significantly impact the MCE and ER calculation for BB smokes in transport region (Yokelson et al., 2013).

In the FT, this issue may not significantly affect the calculation as the background variations of species are likely to be small compared with the excess levels in plumes. FT CO background is calculated to be 78 ppbv (62 μg m^{-3}), which is summarized from the clean FT data (BC < 0.1 μg m^{-3}). The correlation between BC and CO is good (see Table S1) for most of flights. The slopes were determined by the unconstrained ODR fit and are defined as the BC/ΔCO, similar calculation was used for OA/ΔCO. For MCE, the slopes between CO and CO_2 were also determined by the unconstrained ODR fit. The correlation between CO and CO_2 in the FT is good for most of flights (r^2 > 0.8, see Table S1). C036, C037 and C047 are the flights with lower r^2 (~0.70).

In the BL where BB smoke plumes were diluted into a clean environment, the final concentrations were not much greater than the backgrounds, especially for CO_2 which had a high background. It is not suitable for using ODR fit since there is not enough variation in the concentrations to obtain a reliable result. For example, the correlation (r^2 = 0.28—0.88, Table S1) between BC and CO are low for most of flights, and there is not enough variation in CO_2 to obtain a correlation between CO and CO_2. As a result, we did not consider the MCE calculation, since the derived slopes ($\partial CO/\partial CO2$) are misleading and CO and CO_2 concentrations in plume were close to the BL background. In the BL, the background of BC and OA is approximately zero. The lowest 5th percentile for all the BL CO data was 65.8 ppbv and the median of all the clean BL CO data was 66.5 ppbv, BL CO background is calculated to be 66 ppbv (53 μg m^{-3}) by averaging the two results. The background of BL CO was then used to calculate the excess CO (ΔCO), BC/ΔCO and OA/ΔCO ratios.

Table S1. Summary of the flight plume characteristics in the FT and BL separately: flight ID, flight data and r^2 correlation between CO and CO_2, BC and CO and OA and CO.

Flight	Date	CO vs CO_2 r^2	BC vs CO r^2		OA vs CO r^2	
		FT	FT	BL	FT	BL
C028	16/08/2019			0.76		0.04
C029	17/08/2019			0.68		0.49

C030	17/08/2019			0.54		0.48
C031	18/08/2019			0.85		0.83
C032	19/08/2019			0.68		0.70
C033	22/08/2019	0.85	0.89		0.89	
C034	23/08/2019	0.89	0.94		0.93	
C035	23/08/2019	0.94	0.95		0.93	
C036	24/08/2019	0.72	0.88		0.84	
C037	24/08/2019	0.71	0.85		0.83	
C038	25/08/2019	0.86	0.94		0.75	
C039	25/08/2019	0.85	0.94		0.80	
C045	29/08/2019	0.87	0.93	0.27	0.90	0.01
C046	30/08/2019	0.85	0.98	0.74	0.93	0.38
C047	01/09/2019	0.70	0.89	0.49	0.83	0.68
C048	01/09/2019	0.98	0.98	0.53	0.99	0.38
C049	02/09/2019	0.97	0.99	0.71	0.98	0.63
C050	04/09/2019	0.98	0.99	0.61	0.90	0.64
C051	05/09/2019	0.94	0.96	0.88	0.93	0.88

S2 Identification of mostly inorganic nitrate from the AMS

Nitrate is detected in the AMS using peaks at m/z = 30 and 46 (Allan et al., 2003), representing the ions NO^+ and NO_2^+ respectively. The AMS can detect nitrate species including inorganics like NH_4NO_3, $NaNO_3$ and KNO_3, as well as organic nitrates. When sampling different nitrate species, the ratio of these two peaks is determined by the heater temperature and the volatility of nitrate species (Drewnick et al., 2015). Higher ratios were observed for less volatile nitrates, e.g. 28 for KNO_3 and 29.2 for $NaNO_3$, compared to NH_4NO_3, since they decompose further before ionization (Alfarra et al., 2004; Drewnick et al., 2015). Rollins et al. (2010) measured ratios of 1.51 – 5.10 for various organic nitrates. During CLARIFY, the m/z 30 to m/z 46 ratios ranged from 1 to 1.4, from the AMS calibration using mono-disperse NH_4NO_3 particles. The vertical profile of ambient m/z 30 to m/z 46 ratios in CLARIFY FT was shown in Fig. S3. With the C-ToF AMS used in this study, the interference of some ions from organics cannot be separated at these two peaks, such as CH_2O^+, CH_4N^+ and $C_2H_6^+$ at m/z = 30 and $CH_2O_2^+$ and $C_2H_6O^+$ at m/z = 46, which would add uncertainties in the ambient m/z 30 to m/z 46 ratios for nitrate. However, given the small difference between ambient and calibration values, there is likely a low potential interference from large amounts of organic nitrates, and most of observed nitrates would be NH_4NO_3. Furthermore, the linear fitted NH_{4mea}^+/NH_{4neu}^+ ratios (in which NH_{4mea}^+ is the measured ammonium concentration, NH_{4neu}^+ is the calculated ammonium concentration if all acids in the aerosol were neutralized) of FT pollutants in period 2 and 3 were (1.06 ± 0.01) and (1.05 ± 0.02) respectively (Zhang et al., 2007). The ammonium in the FT was sufficient to nearly fully neutralize the aerosol, which further supports our inference that the nitrate measured in the FT was mostly NH_4NO_3.

When the air is sampled into the aircraft inlet, it undergoes a rapid temperature rise before entering the AMS inlet due to ram heating as the air is accelerated on sampling. NH_4NO_3 is a semi-volatile species, and the rapid change in temperature will influence the thermodynamic equilibrium of HNO_3–NH_3–NH_4NO_3 system, causing the evaporation of NH_4NO_3. On the BAe-146 Atmospheric Research Aircraft (ARA), the transport time of sampled air between aircraft inlet and the AMS inlet is ~1–2 s. The timescale for aerosol equilibrium between gas and particle phase is expected to be a few minutes or less under typical polluted conditions (Wexler and Seinfeld, 1992). Therefore, the 1–2 s timescale of heating in the aircraft sampling inlet is sufficiently fast that the partitioning of NH_4NO_3 is not influenced. The observed vertical variation of nitrate mass fraction should reflect the influence of temperature change under ambient conditions, which we discussed in section 4.1.1 in the manuscript.

References

Alfarra, M. R.: Insights into atmospheric organic aerosols using an aerosol mass spectrometer, PhD Thesis, University of Manchester, Institute of Science and Technology, Manchester, UK., 2004.

Allan, J. D., Jimenez, J. L., Williams, P. I., Alfarra, M. R., Bower, K. N., Jayne, J. T., Coe, H., and Worsnop, D. R.: Quantitative sampling using an aerodyne aerosol mass spectrometer – 1. Techniques of data interpretation and error analysis, J. Geophys. Res.- Atmos., 108, 4090, https://doi.org/10.1029/2002JD002358, 2003.

Drewnick, F., Diesch, J.-M., Faber, P., and Borrmann, S.: Aerosol mass spectrometry: particle–vaporizer interactions and their consequences for the measurements, Atmos. Meas. Tech., 8, 3811–3830, https://doi.org/10.5194/amt-8-3811-2015, 2015.

Lefer, B. L., Talbot, R. W., Harriss, R. H., Bradshaw, J. D., Sandholm, S. T., Olson, J. O., Sachse, G. W., Collins, J., Shipham, M. A., Blake, D. R., Klemm, K. I., Klemm, O., Gorzelska, K., and Barrick, J.: Enhancement of acidic gases in biomass burning impacted air masses over Canada, J. Geophys. Res., 99, 1721–1737, https://doi.org/10.1029/93JD02091, 1994.

Rollins, A. W., Fry, J. L., Hunter, J. F., Kroll, J. H., Worsnop, D. R., Singaram, S. W., and Cohen, R. C.: Elemental analysis of aerosol organic nitrates with electron ionization high-resolution mass spectrometry, Atmos. Meas. Tech., 3, 301–310, https://doi.org/10.5194/amt-3-301-2010, 2010.

Wexler, A. S. and Seinfeld, J. H.: Analysis of aerosol ammonium nitrate: departures from equilibrium during SCAQS, Atmos. Environ., 26, 579–591, https://doi.org/10.1016/0960-1686(92)90171-G, 1992.

Yokelson, R. J., Crounse, J. D., DeCarlo, P. F., Karl, T., Urbanski, S., Atlas, E., Campos, T., Shinozuka, Y., Kapustin, V., Clarke, A. D., Weinheimer, A., Knapp, D. J., Montzka, D. D., Holloway, J., Weibring, P., Flocke, F., Zheng, W., Toohey, D., Wennberg, P. O., Wiedinmyer, C., Mauldin, L., Fried, A., Richter, D., Walega, J., Jimenez, J. L., Adachi, K., Buseck, P. R., Hall, S. R., and Shetter, R.: Emissions from biomass burning in the Yucatan, Atmos. Chem. Phys., 9, 5785–5812, https://doi.org/10.5194/acp-9-5785-2009, 2009.

Yokelson, R. J., Andreae, M. O., and Akagi, S. K.: Pitfalls with the use of enhancement ratios or normalized excess mixing ratios measured in plumes to characterize pollution sources and aging, Atmos. Meas. Tech., 6, 2155–2158, https://doi.org/10.5194/amt-6-2155-2013, 2013.

Zhang, Q., Jimenez, J. L., Worsnop, D. R., and Canagaratna, M.: A case study of urban particle acidity and its influence on secondary organic aerosol, Environ. Sci. Technol., 41, 3213–3219, https://doi.org/10.1021/es061812j, 2007.

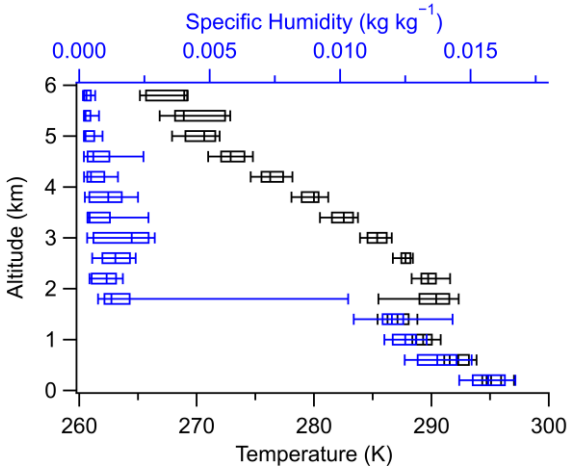

Figure S1: The vertical distribution of temperature (black) and specific humidity (blue) during the campaign. The box-and-whisker plots represent the 10th percentile, 25th percentile, median, 75th percentile and 90th percentile in every 400 m.

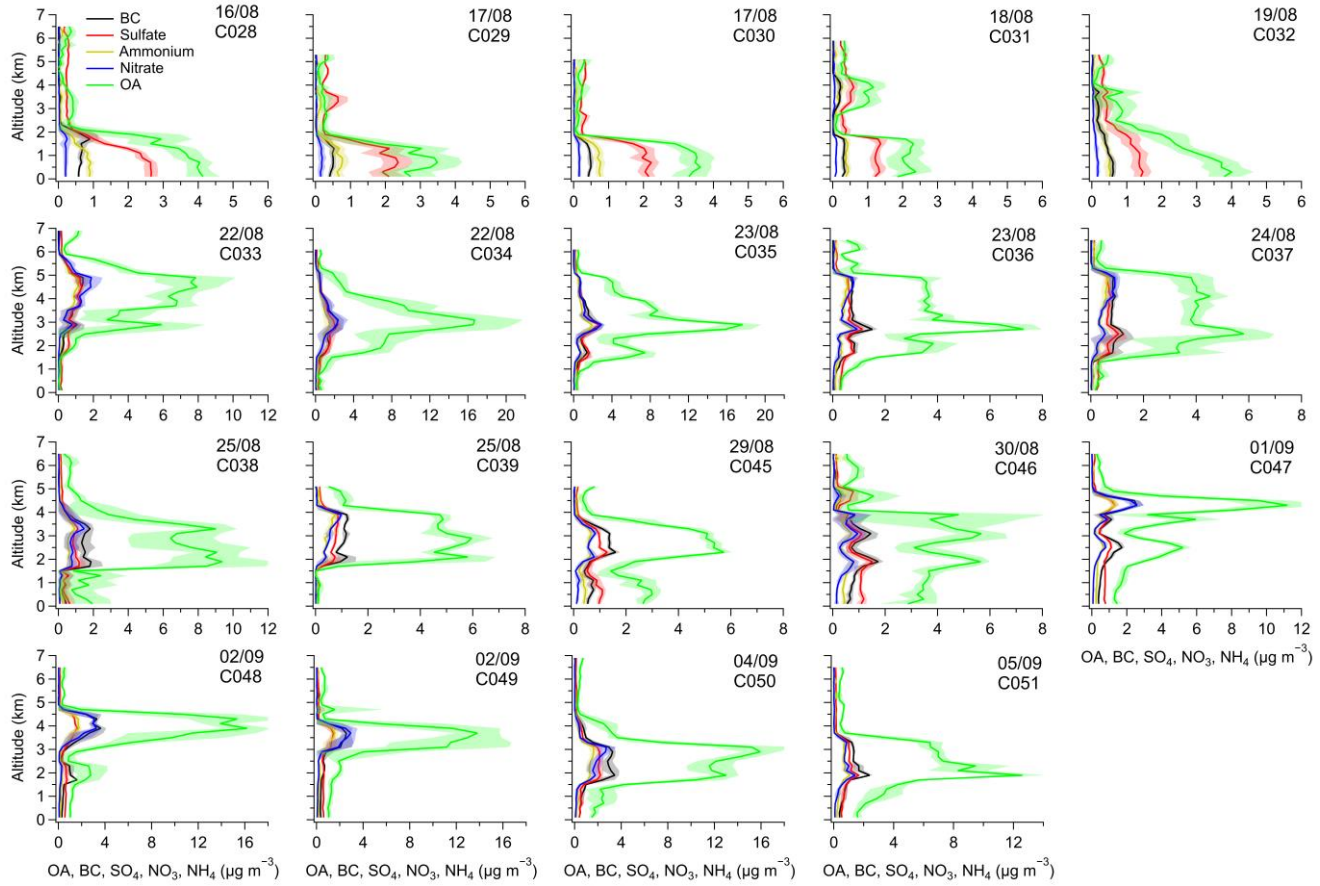

Figure S2: The average vertical distribution of different chemical composition concentrations for each flight. The lines and shades represent the average and standard deviation in every 200 m.

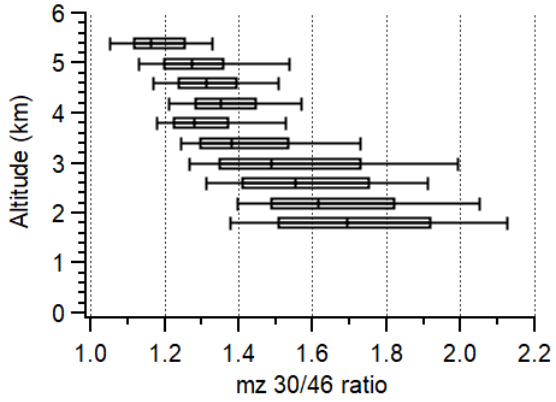

Figure S3: The vertical distribution of m/z 30 over m/z 46 ratios in the BB-polluted FT (from periods 2 and 3). The box-and-whisker plots represent the 10th percentile, 25th percentile, median, 75th percentile and 90th percentile in every 400 m.